Table 6.1: Experimental Rotor Configurations

Configuration	Flap flexure	Lead-lag flexure	Blade pitch angle set
1	nominal, $\omega_{\beta 0} < \omega_{\zeta 0}$	straight, $K_{p\zeta} = 0$	outboard of flexures
2	nominal, $\omega_{\beta 0} < \omega_{\zeta 0}$	skewed, $K_{p\zeta} = -0.4$	outboard of flexures
3	nominal, $\omega_{\beta 0} < \omega_{\zeta 0}$	skewed, $K_{p\zeta} = -0.4$	outboard of flexures
4	thick, $\omega_{\beta 0} = \omega_{\zeta 0}$	straight, $K_{p\zeta} = 0$	outboard of flexures
5	thick, $\omega_{\beta 0} = \omega_{\zeta 0}$	skewed, $K_{p\zeta} = -0.4$	outboard of flexures

Table 6.2: Rotor Structural Properties

Property	Value
Radius, cm	81.10
Chord, cm	4.19
Hinge offset, cm	8.51
Lock number	7.37 (based on $a = 5.73$)
Airfoil	NACA 23012 ($C_0 = 0.15$)
Profile drag (c_{d0})	0.0079
Blade mass (to flap flexure), g	209.00
Blade mass centroid (ref. flexure centerline), cm	18.60
Blade flap inertia (ref. flexure centerline), g-m^2	17.30
Blade polar inertia (ref. hub centerline), g-m^2	85.50

Table 6.3: Blade Frequency and Damping

Configuration	$\omega_{\beta 0}$, Hz	$\omega_{\zeta 0}$, Hz	ξ%
1	3.13	6.70	0.52
2	3.13	7.16	0.65
3	3.13	7.16	0.65
4	6.63	6.73	0.53
5	6.64	7.04	0.65

Table 6.4: Body Properties

Property	Pitch	Roll
Body mass, kg	22.60	19.06
Vertical c.g., cm	1.32	1.56
Body inertia, g-m^2	633.00	183.00

(a) Overall set up of the model

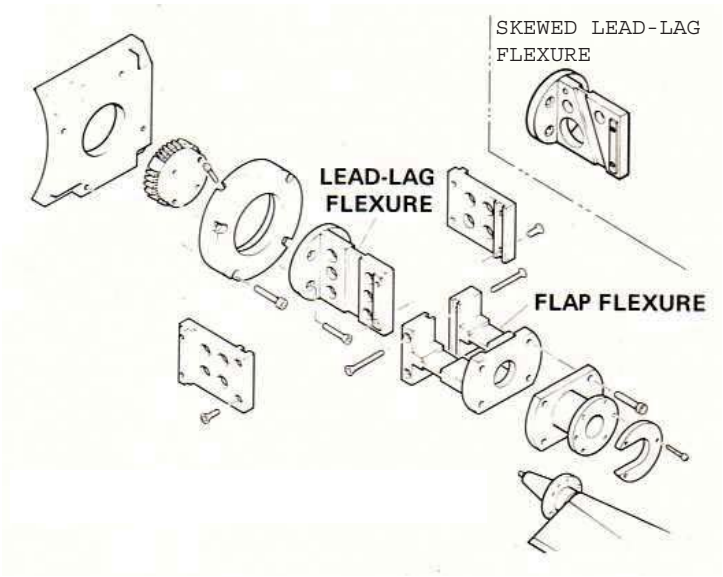

(b) Expanded view of blade root flexures

Figure 6.10: **A 1.62-m diameter, three-bladed model rotor mounted on a static mast**

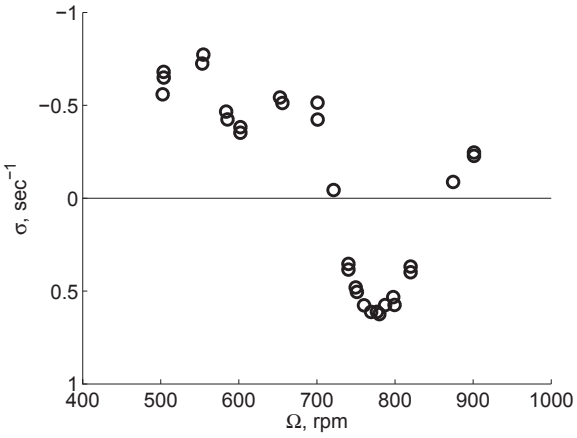

(a) Configuration 1

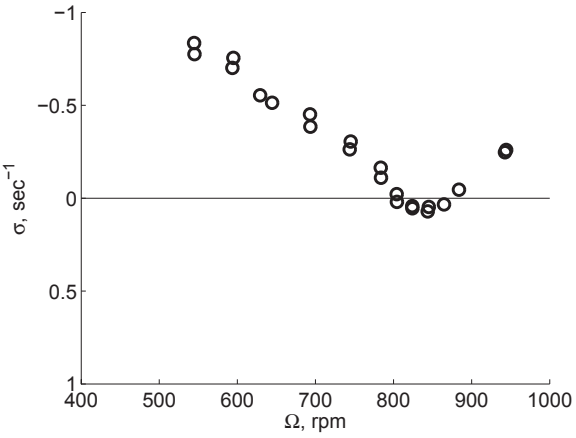

(b) Configuration 2

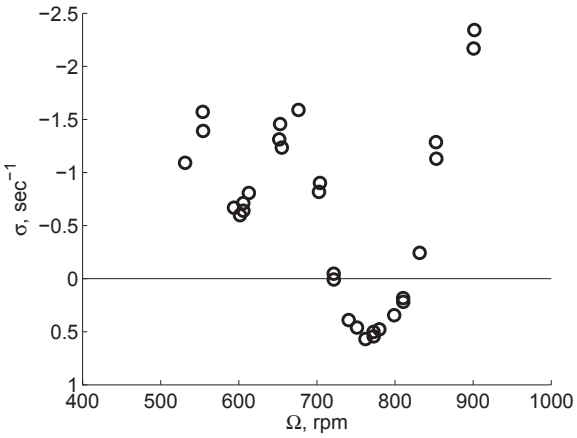

(c) Configuration 3

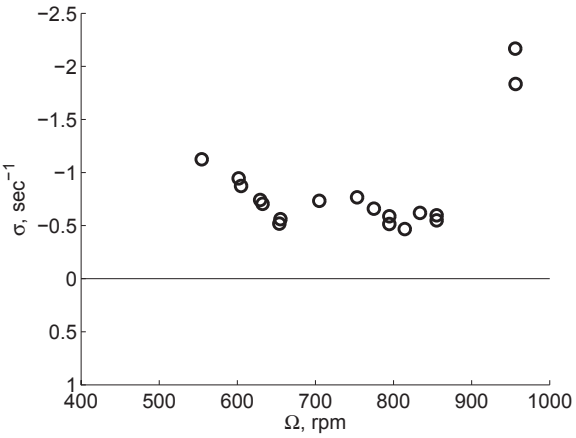

(d) Configuration 4

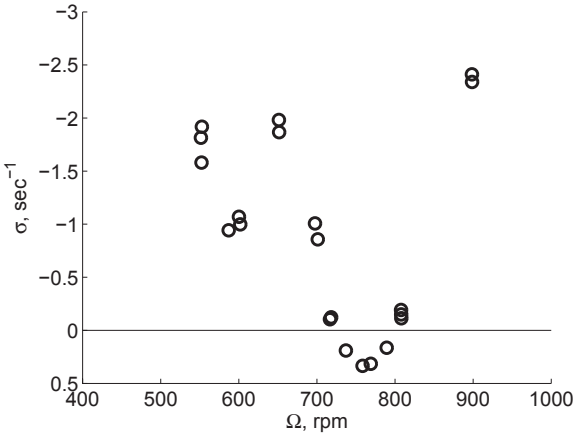

(e) Configuration 5

Figure 6.11: **Lead-lag regressing mode damping as a function of rotor speed at blade pitch angle $\theta_0 = 9^o$**

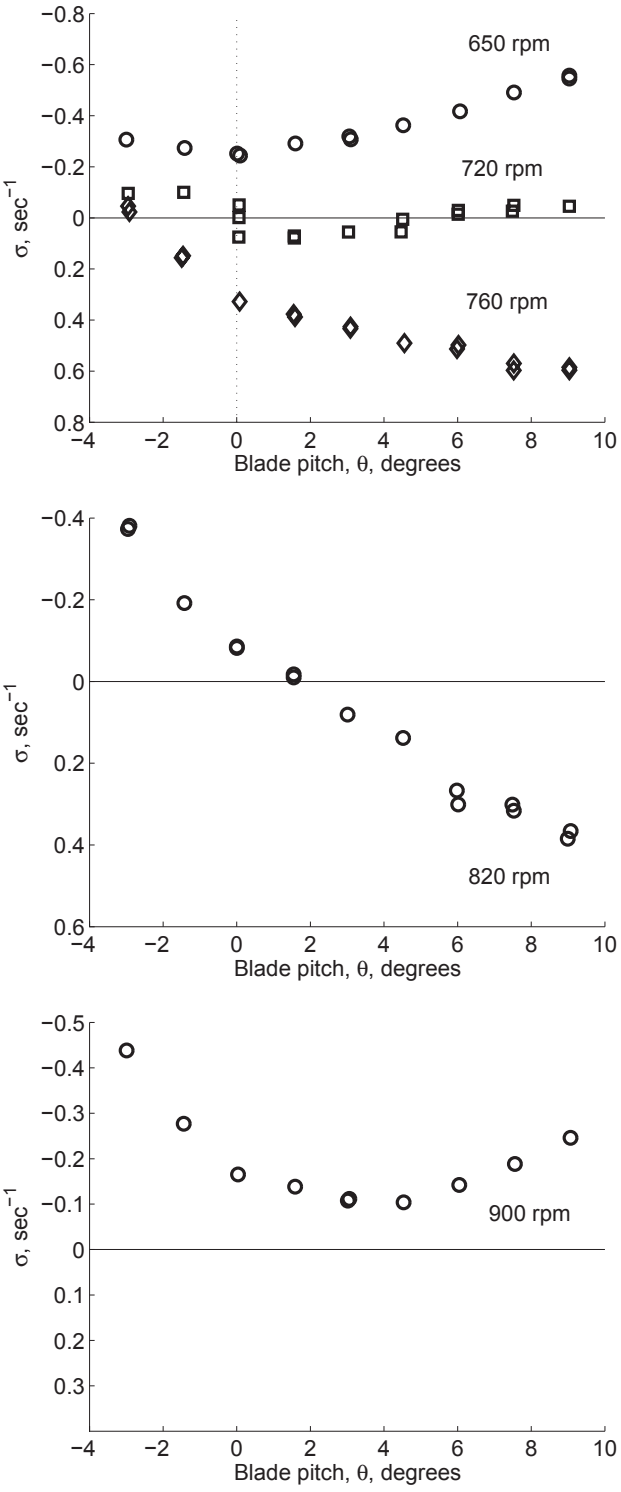

Figure 6.12: **Lead-lag regressing mode damping as a function of blade pitch angle for configuration 1;** $\omega_{\beta 0} < \omega_{\zeta 0}$**,** $K_{p\zeta} = 0$

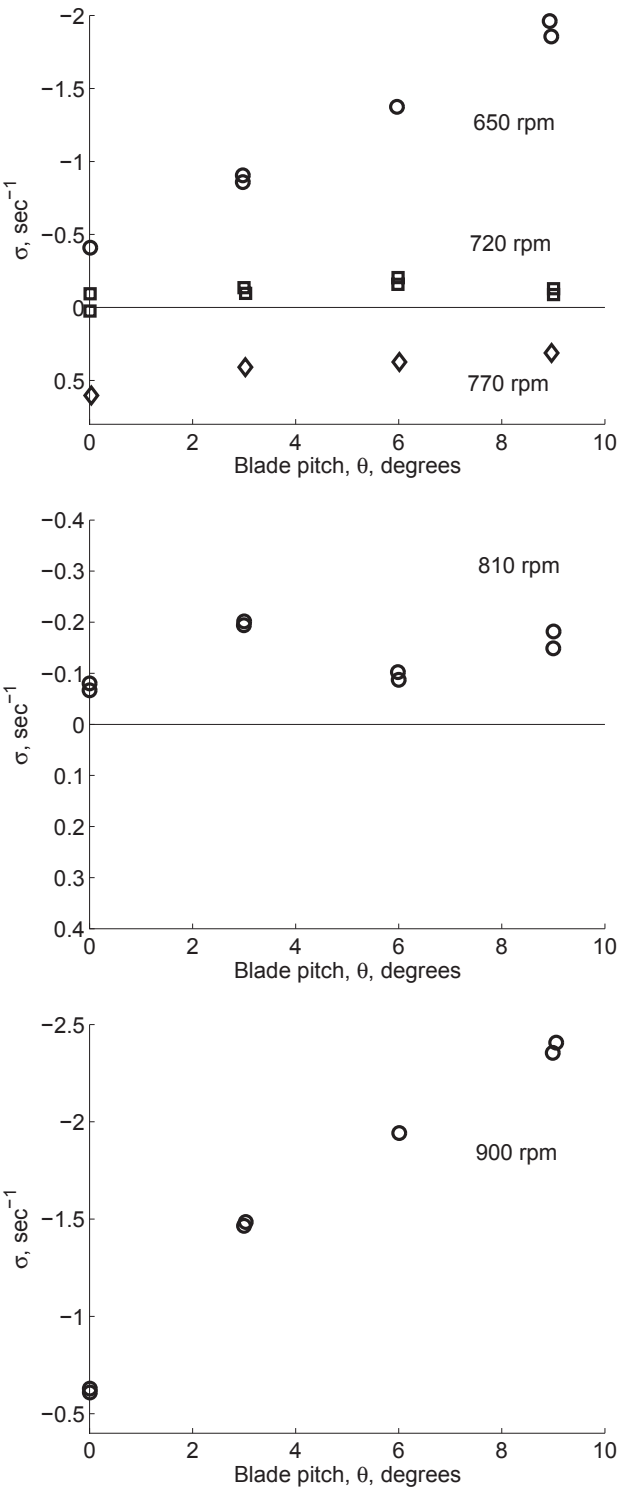

Figure 6.13: **Lead-lag regressing mode damping as a function of blade pitch angle for configuration 3;** $\omega_{\beta 0} < \omega_{\zeta 0}$**,** $K_{p\zeta} = -0.4$

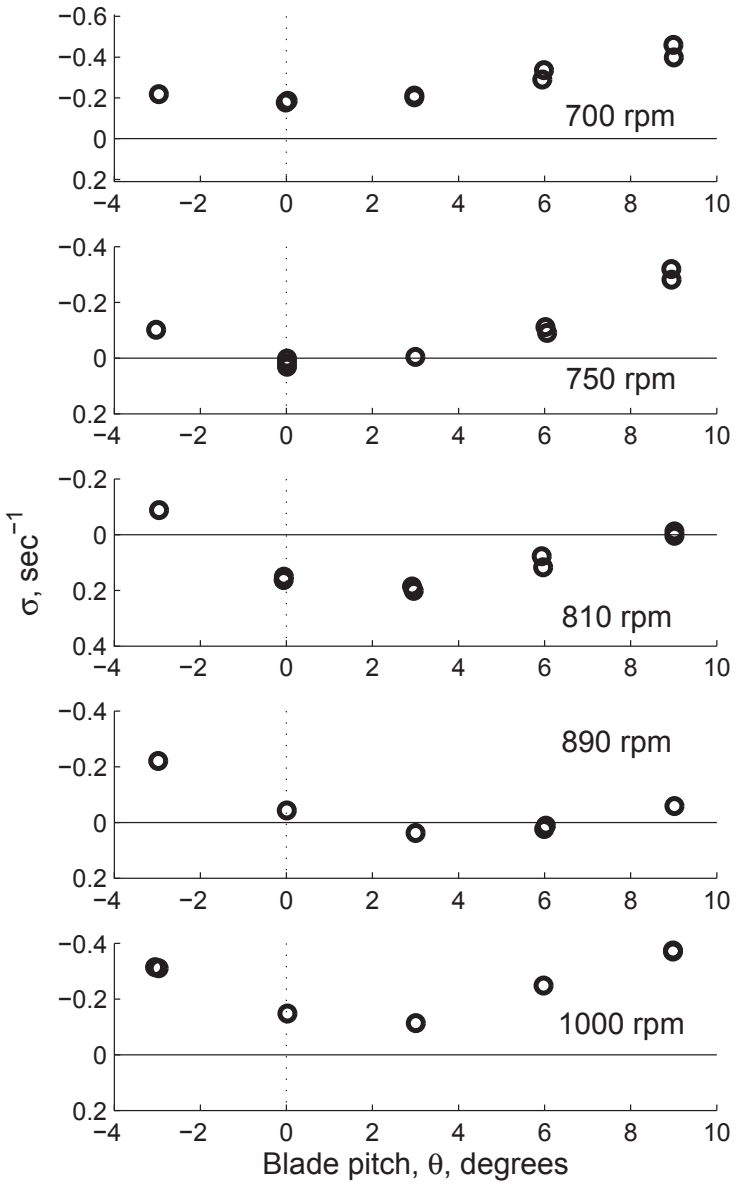

Figure 6.14: **Lead-lag regressing mode damping as a function of blade pitch angle for configuration 4;** $\omega_{\beta 0} = \omega_{\zeta 0}$**,** $K_{p\zeta} = 0$

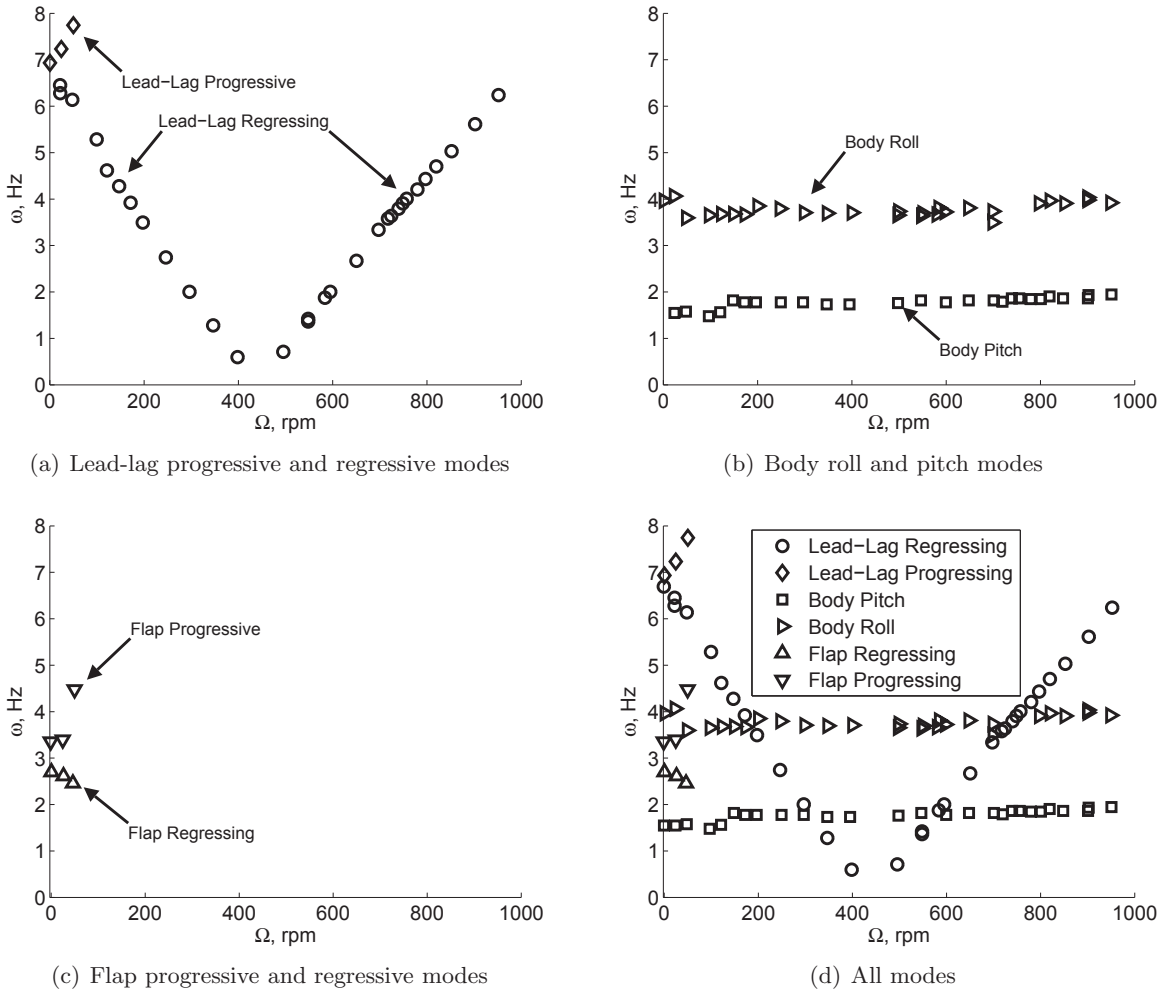

(a) Lead-lag progressive and regressive modes

(b) Body roll and pitch modes

(c) Flap progressive and regressive modes

(d) All modes

Figure 6.15: **Modal frequencies as a function of rotor speed for configuration 1;** $\omega_{\beta 0} < \omega_{\zeta 0}$**,** $K_{p\zeta} = 0$**, blade pitch angle** $theta_b = 0$

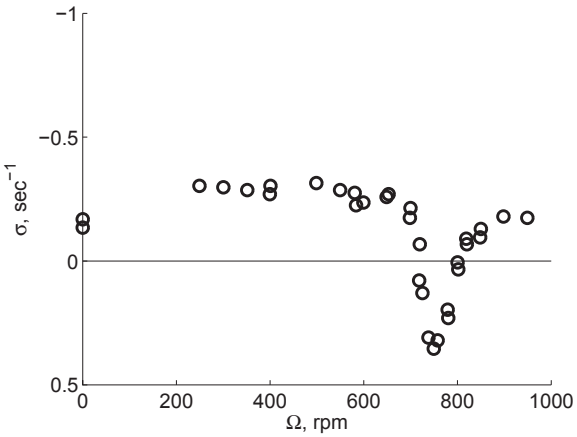

(a) Lead-lag regressive mode damping

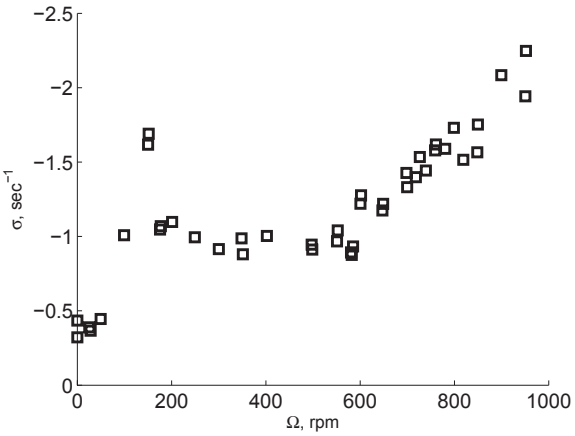

(b) Body pitch mode damping

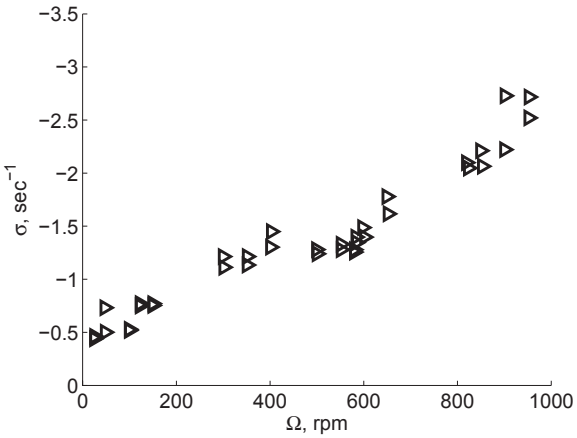

(c) Body roll mode damping

Figure 6.16: **Modal damping as a function of rotor speed for configuration 1;** $\omega_{\beta 0} < \omega_{\zeta 0}$**,** $K_{p\zeta} = 0$**.**

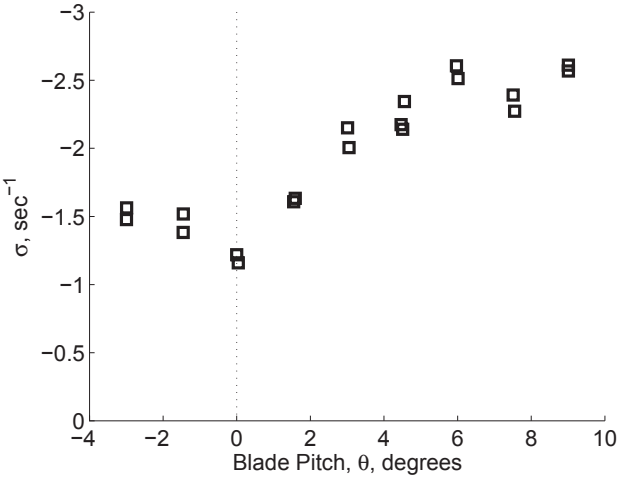

(a) Body pitch mode damping

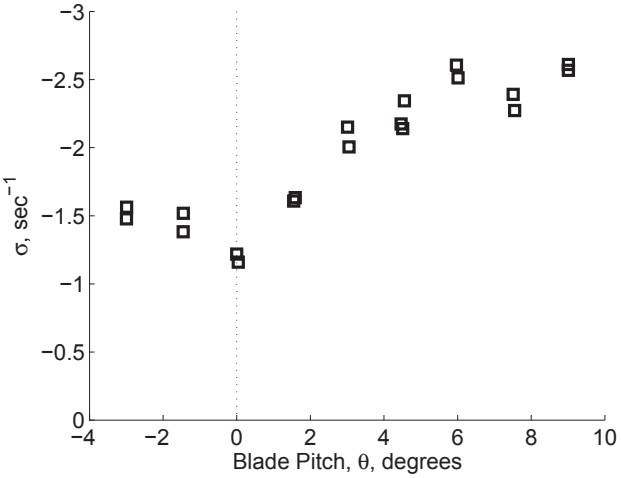

(b) Body roll mode damping

Figure 6.17: **Body pitch and roll mode damping as a function of blade pitch angle for configuration 1;** $\omega_{\beta 0} < \omega_{\zeta 0}$**,** $K_{p\zeta} = 0$**,** $\Omega = 650$ **rpm.**

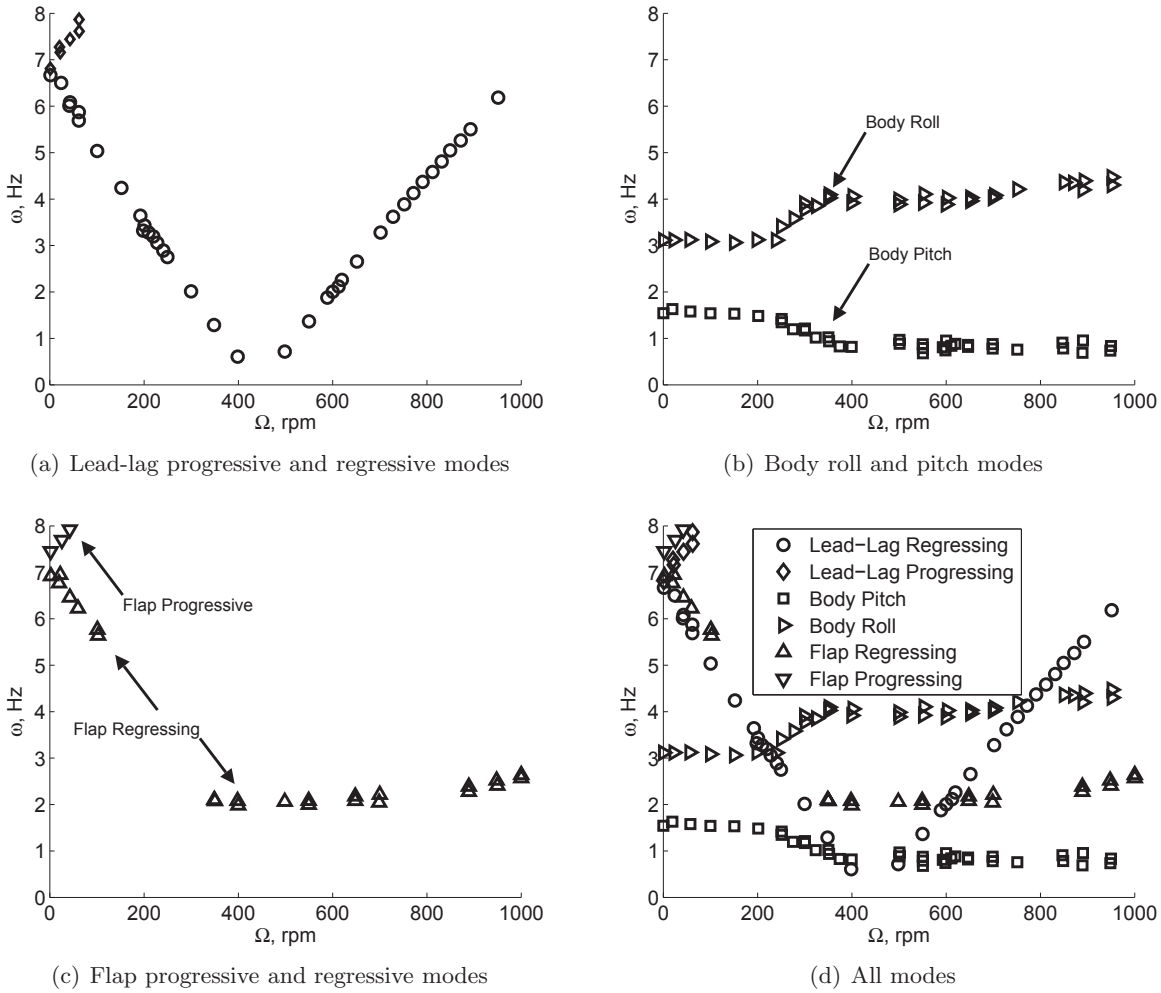

(a) Lead-lag progressive and regressive modes

(b) Body roll and pitch modes

(c) Flap progressive and regressive modes

(d) All modes

Figure 6.18: **Modal frequencies as a function of rotor speed for configuration 4;** $\omega_{\beta 0} = \omega_{\zeta 0}$**,** $K_{p\zeta} = 0$**, blade pitch angle** $\theta_b = 0$**.**

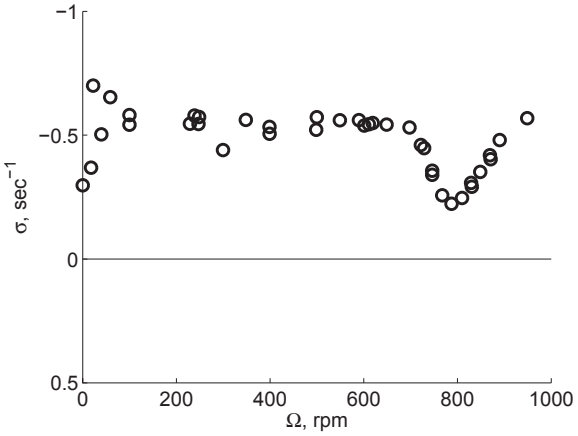

(a) Lead-lag regressive mode damping

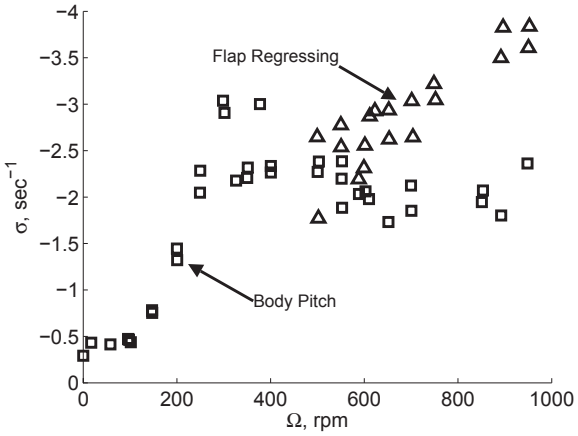

(b) Body pitch and flap regressive mode damping

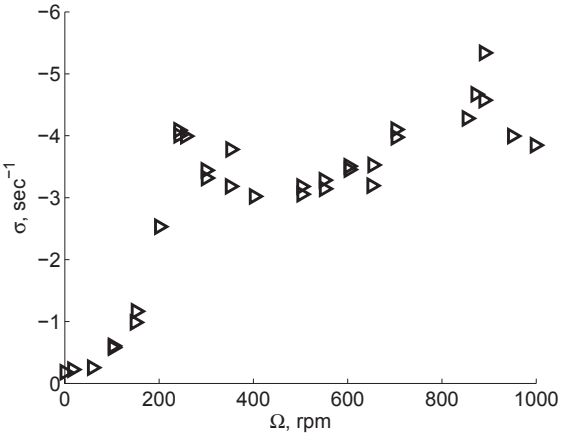

(c) Body roll mode damping

Figure 6.19: **Modal damping as a function of rotor speed for configuration 1;** $\omega_{\beta 0} < \omega_{\zeta 0}$**,** $K_{p\zeta} = 0$**.**

Bibliography

[1] Coleman, R. P. and Feingold, A. M., "Theory of Self-Excited Mechanical Oscillations of Helicopter Rotors with Hinged Blades," NACA Report 1351, 1958.

[2] Hammond, C. E., "An applicatoin of Floquet theory to the prediction of mechanical instability," Journal of the American Helicopter Society, Vol. 19, No.4, Oct. 1974. pp, 14-23.

[3] Bousman, W. G., "An Experimental Investigation of the Effects of Aeroelastic Couplings on Aeromechanical Stability of a Hingeless Rotor Helicopter," *Journal of the American Helicopter Society*, Vol. 26, (1), January 1981, pp. 46–54.

[4] Donham, R. E., Cardinale, S. V., and Sachs, I. B., "Ground and Air Resonance Characteristics of a Soft In-plane Rigid-Rotor System," *Journal of the American Helicopter Society*, Vol. 14, (4), October 1969, pp. 33–41.

[5] Lytwyn, R. T., Miao, W., and Woitsch, W., "Airborne and Ground Resonance of Hingeless Rotors," *Journal of the American Helicopter Society*, Vol. 16, (2), April 1971, pp. 2–9.

[6] Miao, W., Edwards, W. T., and Brandt, D. E., "Investigation of Aeroelastic Stability Phenomena of the Helicopter by In-flight Shake Test," *NASA Symposium on Flutter Testing Techniques*, NASA SP-415, 1976, pp. 473–495.

[7] Staley, J. A., Gabel, R., and MacDonald, H. I., "Full Scale Ground and Air Resonance Testing of the Army-Boeing Vertol Bearingless Main Rotor," Preprint No. 79–23. American Helicopter Society 35th Annual Forum Proceedings, May 1979.

Chapter 7

Aeroelastic Stability in Forward Flight

The forward flight condition introduces an extra dimension of complexity to the rotorcraft aeroelastic stability and response problems. The airflow on the disk is asymmetric, and also a part of the region is in either stalled flow or in reversed flow condition. The complexity is caused by the blade aerodynamic forces which are very much involved.

The equations of blade motion in forward flight contain many periodic terms and therefore one has to develop special mathematical tools to solve these equations. One possible way of solving these equations is to write the blade equations in the fixed reference frame using Fourier coordinate transformation, and then solve these equations approximately either neglecting altogether periodic terms or using the harmonic balance method on the periodic terms. The other involved method is to use Floquet theory in the fixed reference frame. The second approach is to keep the blade equations in the rotating reference frame and solve these using the Floquet or time integration technique or harmonic balance method. With the dynamic inflow modeling, it is more appropriate to use the first approach and solve the equations in the fixed reference frame.

To understand the fundamentals of forward flight, we shall start with a simple blade model undergoing rigid flap motion. Later on a two-degree-of-motion, flap and lag, will be investigated for aeroelastic stability in forward flight.

7.1 Flap Motion in forward flight

The blade is assumed rigid and it undergoes a single degree of motion, rigid flap, about the flap hinge. The blade is exposed to forward flight environment.

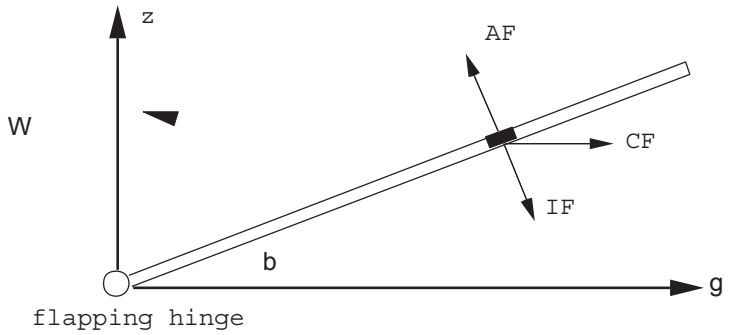

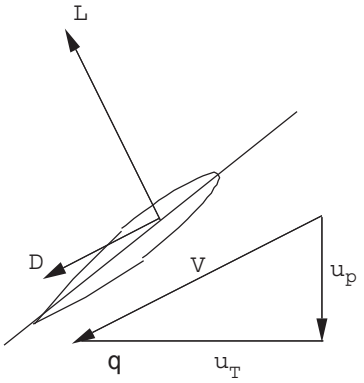

The equation of motion of a blade is

$$\overset{**}{\beta} + \nu_\beta^2 \beta = \gamma \overline{M}_\beta$$

where ν_β is the rotating flap frequency and γ is the Lock number. The $\overline{M}_\beta$ represents the aerodynamic moment about the flap hinge

$$\overline{M}_\beta = \frac{1}{\rho a c \Omega^2 R^4} \int_0^L r\, F_z\, dr$$

$$F_z \approx L$$

$$= \frac{1}{2}\rho V^2 c a (\theta - \frac{u_p}{u_T})$$

$$= \frac{1}{2}\rho c a (u_t^2 \theta - u_p u_T)$$

The flow components are

$$\frac{u_T}{\Omega R} = \mu \sin\psi + x$$

$$\frac{u_p}{\Omega R} = x\dot{\beta} + \lambda + \beta\mu\cos\psi$$

where $x = \frac{r}{R}$ and λ is the induced inflow. The μ is the advance ratio,

$$\mu = \frac{v\cos\alpha}{\Omega R} \approx \frac{V}{\Omega R} \quad \text{(a is tilt of TPP)}$$

$$\overline{M}_\beta = \frac{1}{2}\int_0^1 x \left[\left(\frac{u_T}{\Omega R}\right)^2 \theta - \frac{u_p}{\Omega R}\frac{u_T}{\Omega R} \right] dx$$

Assuming θ is uniform along the blade length. It is also assumed that the induced inflow λ is uniform on the disk.

$$\overline{M}_\beta = \left(\frac{1}{8} + \frac{\mu}{3}\sin\psi + \frac{\mu^2}{4}\sin^2\psi\right)\theta - \left(\frac{1}{8} + \frac{\mu}{6}\sin\psi\right)\overset{*}{\beta}$$

$$- \left(\frac{1}{6} + \frac{\mu}{4}\sin\psi\right)\lambda - \mu\cos\psi\left(\frac{1}{6} + \frac{\mu}{4}\sin\psi\right)\beta$$

The flap equation becomes

$$\overset{**}{\beta} + \left(\frac{1}{8} + \frac{\mu}{6}\sin\psi\right)\overset{*}{\beta} + \left[\nu_\beta^2 + \gamma\mu\cos\psi\left(\frac{1}{6} + \frac{\mu}{4}\sin\psi\right)\right]\beta$$

$$= \gamma \left(\frac{1}{8} + \frac{\mu}{3} \sin\psi + \frac{\mu^2}{4} \sin^2\psi \right) \theta$$

$$-\gamma \left(\frac{1}{6} + \frac{\mu}{4} \sin\psi \right) \lambda \tag{7.1}$$

This is a linear differential equation containing periodic coefficients. If the effect of pitch-flap coupling k_{p_β} is also to be introduced, then replace θ by $\theta - k_{p_\beta}$ in the above equation.

$$\overset{**}{\beta} + \gamma \left(\frac{1}{8} + \frac{\mu}{6} \sin\psi \right) \overset{*}{\beta} + \left[\nu_\beta^2 + \gamma\mu \cos\psi \left(\frac{1}{6} + \frac{\mu}{4} \sin\psi \right) \right.$$

$$\left. + \gamma \left(\frac{1}{8} + \frac{\mu}{3} \sin\psi + \frac{\mu^2}{4} \sin^2\psi \right) k_{p_\beta} \right] \beta$$

$$= \gamma \left(\frac{1}{8} + \frac{\mu}{3} \sin\psi + \frac{\mu^2}{4} \sin^2\psi \right) \theta - \gamma \left(\frac{1}{6} + \frac{\mu}{4} \sin\psi \right) \lambda \tag{7.2}$$

7.2 Hover Stability Roots

Let us first examine hover flight case ($\mu = 0$). The blade equation becomes

$$\overset{**}{\beta} + \frac{\gamma}{8} \overset{*}{\beta} + \left(\nu_\beta^2 + \frac{\gamma}{8} k_{p_\beta} \right) \beta = \frac{\gamma\theta}{8} - \frac{\gamma\lambda}{6}$$

The stability of the system can be examined from the eigenvalues of this equation.

$$s = -\frac{\gamma}{16} \pm i \sqrt{\nu_\beta^2 + k_{p_\beta} \frac{\gamma}{8} - \left(\frac{\gamma}{16} \right)^2}$$

This is a complex pair i.e., two eigenvalues. The real part of the eigenvalue represents the damping of the flap mode and the imaginary part represents the frequency of the flap mode.

Frequency of damped oscillations $\omega_d = \sqrt{\nu_\beta^2 + k_{p_\beta} \frac{\gamma}{8} - \left(\frac{\gamma}{16} \right)^2}$

Natural frequency $\nu_{\beta_e} = \sqrt{\nu_\beta^2 + k_{p_\beta} \frac{\gamma}{8}}$

Damping ratio $\zeta = -\frac{\text{Real } s}{|s|}$

$$= \frac{\gamma}{16 \nu_{\beta_e}}$$

Thus, the damping of the flap mode depends on the Lock number and is always a positive number. This shows that there is no likelihood of instability of the flap mode. In fact, for a typical Lock number of 8, the damping ratio is about 50%, a very high number. This damping is due to aerodynamic force caused by the flapping motion. For a 4-bladed rotor, there will be four identical pairs. Let us plot roots for a blade in a complex plane

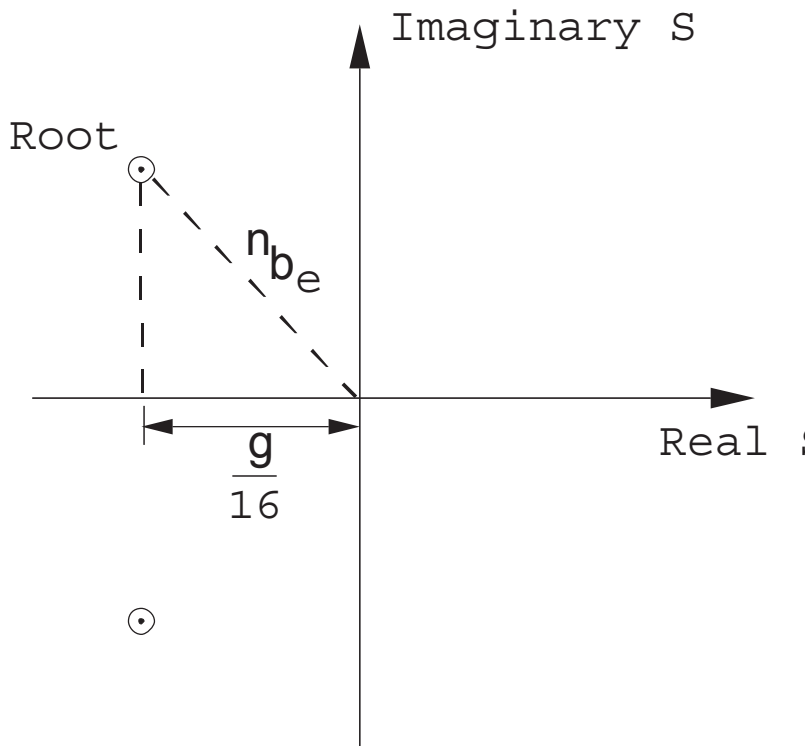

The roots will always lie in the left half of the plane on a semi-circular arc.

7.3 Forward Flight Stability Roots

The equation of motion for a blade in forward flight (Eq. 7.2) contains periodic coefficients. This equation is expressed in the rotating reference frame. One way is to solve numerically this equation using the Floquet theory. For hover case ($\mu = 0$), the roots are complex conjugate pairs and the magnitude of the root depends on ν_β, Y and k_{p_β}. For forward flight the roots, in addition, also depend on the advance ratio, μ. For low μ, the forward flight roots behavior is influenced by hover roots. Let us consider these blade cases with $k_{p_\beta} = 0$.

I. $\nu_\beta = 1$ and $\gamma = 12$ (Articulated)

$$s_{\text{hover}} = -\frac{12}{16} \pm i\sqrt{1 - (\frac{12}{16})^2}$$

$$= -\frac{3}{4} \pm i\sqrt{\frac{7}{16}}$$

Frequency of oscillation close to 1/2 per rev.

II. $\nu_\beta = 1.15$ and $\gamma = 6$ (Hingeless)

$$s_{\text{hover}} = -\frac{3}{8} \pm i\sqrt{(1.15)^2 - \frac{9}{64}}$$

Frequency of oscillation close to 1 per rev.

III. $\nu_\beta = 1.0$ and $\gamma = 6$ (Articulated)

$$s_{\text{hover}} = -\frac{3}{8} \pm i\sqrt{1 - \frac{9}{64}}$$

Frequency of oscillation not close to 1/2 per rev. or 1 per rev.

Let us examine the behavior of roots for change of μ from 0 to 0.5.

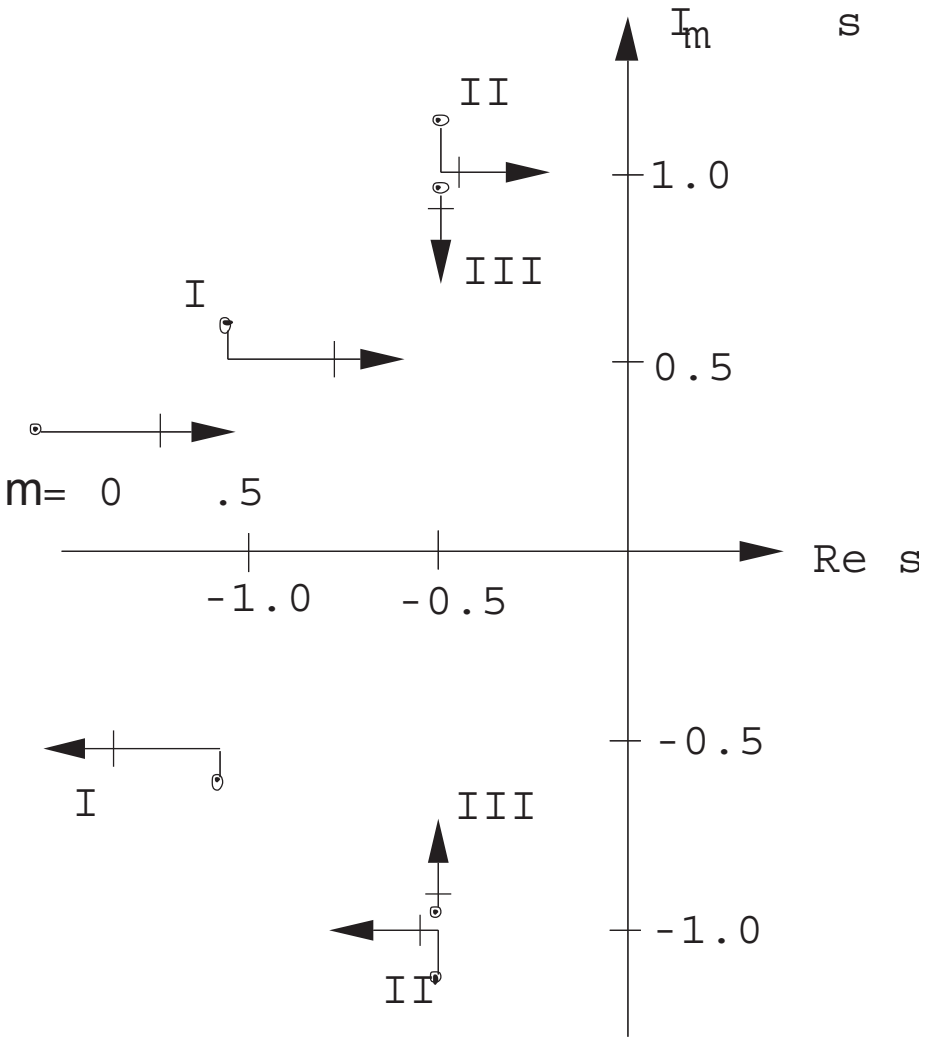

For values of γ and ν_β such that the hover frequency ($I_m s$) is not close to a multiple of 1/2/rev. (Case III), the roots for low μ only exhibit a second order (μ^2) change in frequency and the damping remains unchanged.

For values of γ and ν_β such that the hover frequency ($I_m s$) is close to a multiple of 1/2/rev. (Case I), the roots for low μ exhibit a first order (μ) change. There can occur a degradation of stability, perhaps even an instability, an important characteristic of the periodic system.

For values of γ and ν_β such that the hover frequency ($I_m s$) is close to 1/rev. (Case II), the roots exhibit similar behavior like Case I. For both cases one finds that the frequency $I_m s$ decreases while damping Real s remains constant until an integer multiple of 1/2/rev. is reached. A further increase of μ results in a change of damping, a decrease for the upper root and an increase for the lower root, and the frequency stays constant. For larger μ, one needs to include the effect of reversed flow as well as higher modes.

7.3.1 Stability Roots in Rotating Coordinates

7.3.2 Stability Roots in Fixed Coordinates

Let us examine the flapping dynamics in the fixed reference frame. The equation of motion for the blade flapping in the rotating frame (Eq. 7.2) is converted to the fixed reference frame using the Fourier coordinate transformation.

Let us consider a 3-bladed rotor, n = 1

$$\beta^{(m)} = \beta_0 + \beta_{1c}\cos\psi_m + \beta_{1s}\sin\psi_m$$

Using

$$\frac{1}{N}\sum_{m=1}^{N}(de) = 0$$

$$\frac{2}{N}\sum_{m=1}^{N}(de)\cos\psi_m = 0$$

$$\frac{2}{N}\sum_{m=1}^{N}(de)\sin\psi_m = 0$$

results in

$$\begin{bmatrix} \overset{**}{\beta}_0 \\ \overset{**}{\beta}_{1c} \\ \overset{**}{\beta}_{1s} \end{bmatrix} = \begin{bmatrix} \frac{\gamma}{8} & 0 & \frac{\mu\gamma}{12} \\ 0 & \frac{\gamma}{8}+\frac{\mu\gamma}{12}\sin 3\psi & 2-\frac{\mu\gamma}{12}\cos 3\psi \\ \frac{\mu\gamma}{6} & -2-\frac{\mu\gamma}{12}\cos 3\psi & \frac{\gamma}{8}-\frac{\mu\gamma}{12}\sin 3\psi \end{bmatrix} \begin{bmatrix} \overset{*}{\beta}_0 \\ \overset{*}{\beta}_{1c} \\ \overset{*}{\beta}_{1s} \end{bmatrix}$$

$$+ \begin{bmatrix} \nu_\beta^2 & \frac{\mu^2\gamma}{16}\sin 3\psi & -\frac{\mu^2\gamma}{16}\cos 3\psi \\ \frac{\mu\gamma}{6}+\frac{\mu^2\gamma}{8}\sin 3\psi & \nu_\beta^2-1+\frac{\mu\gamma}{6}\cos 3\psi & \frac{\gamma}{8}+\frac{\mu\gamma}{6}\sin 3\psi+\frac{\mu^2\gamma}{16} \\ -\frac{\mu^2\gamma}{8}\cos 3\psi & -\frac{\gamma}{8}+\frac{\mu^2\gamma}{16}+\frac{\mu\gamma}{6}\sin 3\psi & \nu_\beta^2-1-\frac{\mu\gamma}{6}\cos 3\psi \end{bmatrix} \begin{bmatrix} \beta_0 \\ \beta_{1c} \\ \beta_{1s} \end{bmatrix} \tag{7.3}$$

Similarly for a 4-bladed rotor

$$\beta^{(m)} = \beta_0 + \beta_{1c}\cos\psi_m + \beta_{1s}\sin\psi_m + \beta_2(-1)^{(m)}$$

results in

$$\begin{bmatrix} \overset{**}{\beta}_0 \\ \overset{**}{\beta}_{1c} \\ \overset{**}{\beta}_{1s} \\ \overset{**}{\beta}_2 \end{bmatrix} = \begin{bmatrix} \frac{\gamma}{8} & 0 & \frac{\mu\gamma}{12} & 0 \\ 0 & \frac{\gamma}{8} & 2 & \frac{\mu\gamma}{6}\sin 2\psi \\ -\frac{\mu\gamma}{16} & -2 & \frac{\gamma}{8} & -\frac{\mu\gamma}{6}\cos 2\psi \\ 0 & \frac{\mu\gamma}{12}\sin 2\psi & -\frac{\mu\gamma}{12}\cos 2\psi & \frac{\gamma}{8} \end{bmatrix} \begin{bmatrix} \overset{*}{\beta}_0 \\ \overset{*}{\beta}_{1c} \\ \overset{*}{\beta}_{1s} \\ \overset{*}{\beta}_2 \end{bmatrix} +$$

$$\begin{bmatrix} \nu_\beta^2 & 0 & 0 & \frac{\mu^2\gamma}{8}\sin 2\psi \\ \frac{\mu\gamma}{6} & \nu_\beta^2-1+\frac{\mu^2\gamma}{16}\sin 4\psi & \frac{\gamma}{8}+\frac{\gamma}{16}\mu^2-\frac{\gamma}{16}\mu^2\cos 4\psi & \frac{\mu\gamma}{6}\cos 2\psi \\ 0 & -\frac{\gamma}{8}+\frac{\gamma}{16}\mu^2-\frac{\gamma}{16}\mu^2\cos 4\psi & \nu_\beta^2-1-\mu^2\frac{\gamma}{16}\sin 4\psi & \frac{\mu\gamma}{8}\sin 2\psi \\ \frac{\mu^2\gamma}{8}\sin 2\psi & \frac{\mu\gamma}{6}\cos 2\psi & \frac{\mu\gamma}{6}\sin 2\psi & \nu^2\beta \end{bmatrix} \begin{bmatrix} \beta_0 \\ \beta_{1c} \\ \beta_{1s} \\ \beta_2 \end{bmatrix} \tag{7.4}$$

It is important to note that the 3-bladed rotor equations in the fixed system contain periodic terms of 3ψ only. For a 4-bladed rotor, the equations contain periodic terms of 4ψ as well as 2ψ. Therfore, in the fixed system, the vibratory forces take place at N/rev for an odd bladed rotor and N/rev and $\frac{\mathrm{N}}{2}$/rev for an even bladed rotor where N is the tortal number of blades.

Let us examine an example of an articulated 3-bladed rotor with $\nu_\beta = 1$ and $\gamma = 12$. In the rotating frame there are three identical roots

$$s_R = -\frac{3}{4} \pm \sqrt{\frac{7}{16}}$$

and in the fixed systems, again there are three roots;

coning $s = s_R$

high frequency $s = s_R + i$

low frequency $s = s_R - i$

For forward flight condition, the roots of the equations can be obtained for different μ. One simple approach is to neglect all periodic terms in the fixed system equations and solve these as constant coefficient equations. The results are quite satisfactory for low advance ratios ($\mu < 0.5$), expecially for the low frequency mode. One should keep in mind that this type of approximation won't work in the rotating frame. The second method is to solve the fixed frame equations numerically using the Floquet theory. Another way is to use the harmonic balance method in the fixed frame. In the figure, results are obtained using the Floquet theory and constant coefficient approximation.

The stability behavior will be identical whether the rotating reference frame or the fixed reference frame are used.

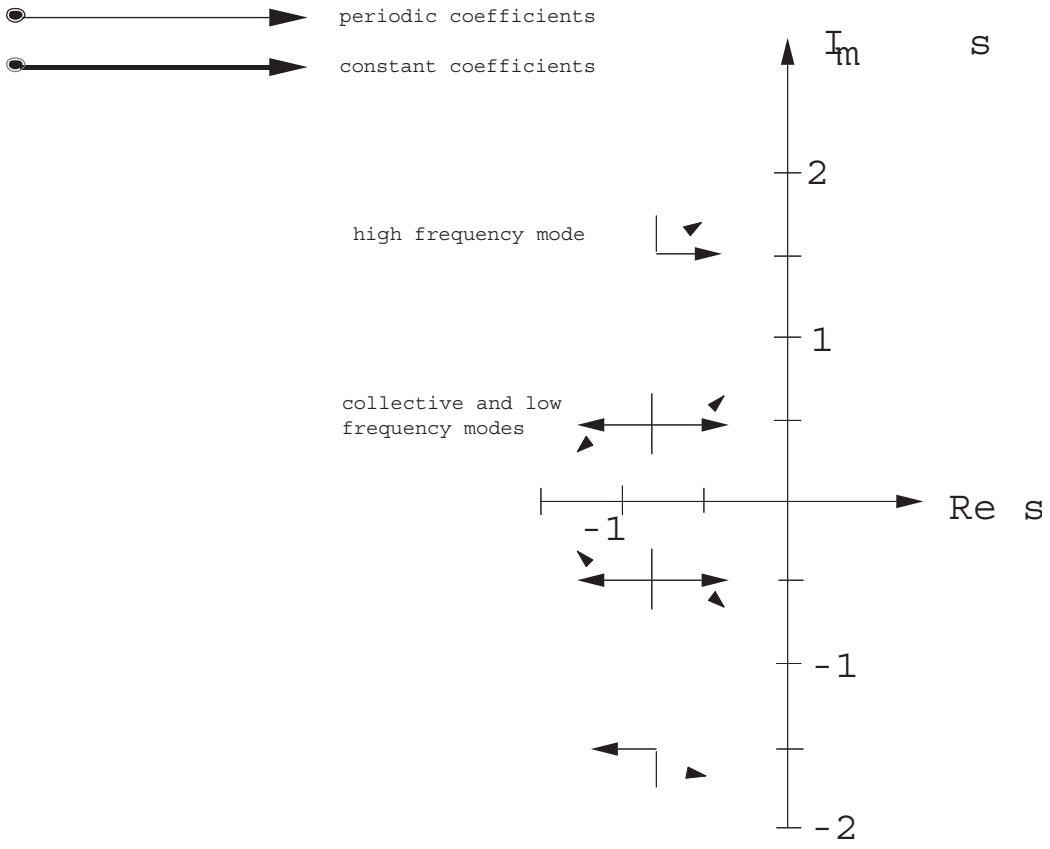

7.4 Flap-lag Stability in Forward Flight

The blade is assumed rigid and it undergoes two degrees of motion, flap and lag motions about hinges. There are bending springs at the hinges to obtain desired flap and lag frequencies.

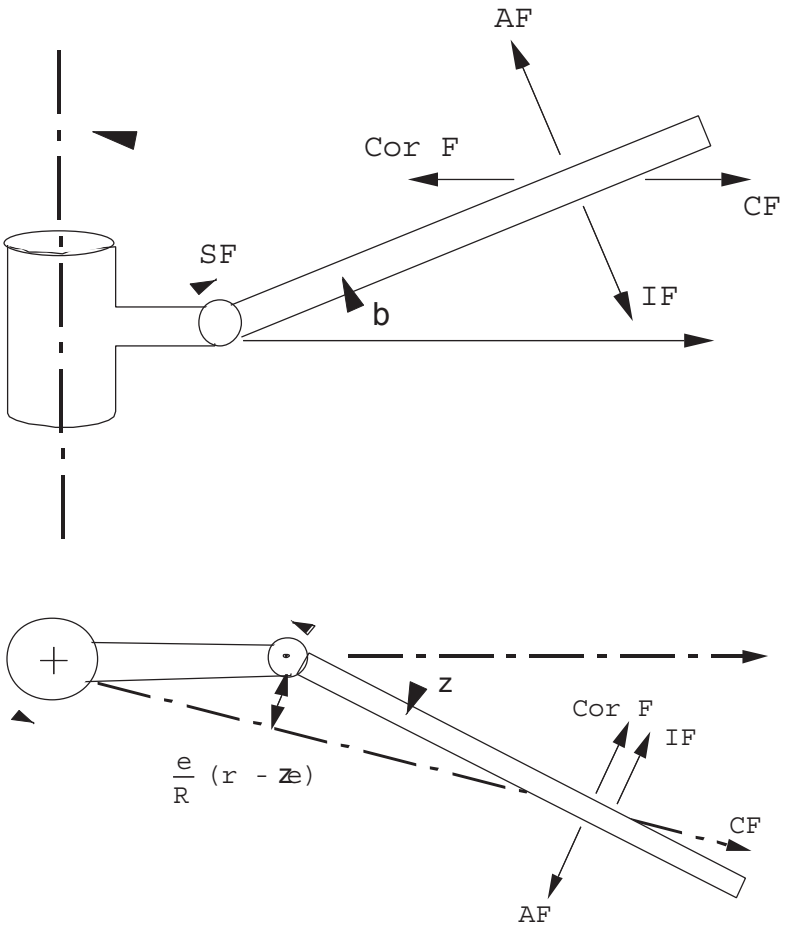

The equations of motion become

$$
\begin{aligned}
&\text{Flap Eq.:}\\
&\overset{**}{\beta} + \nu_\beta^2 \beta - 2\beta \overset{*}{\zeta} = \gamma \overline{M}_\beta + \frac{\omega_{\beta 0}^2}{\Omega^2}\beta_p\\
&\text{Lag Eq.:}\\
&\overset{**}{\zeta} + \nu_\zeta^2 \zeta + 2\frac{\omega_{\zeta 0}}{\Omega}\zeta_L \overset{*}{\zeta} + \beta \overset{*}{\beta} = \gamma \overline{M}_\zeta
\end{aligned}
\tag{7.5}
$$

where ν_β and ν_ζ are rotating flap and lag frequencies and ζ_L is the structural damping coefficient in the lag mode. The ω_{β_0} and ω_{ζ_0} are the nonrotating flap and lag frequencies.

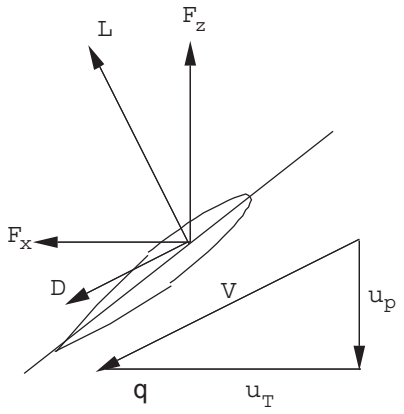

Quasisteady aerodynamics is used to obtain the aerodynamic forces on the blade. The reversed flow effects are neglected.

$$F_z \approx L = \frac{1}{2}\rho ac\left(u_T^2\theta - u_p u_T\right)$$

$$F_x \approx L\frac{u_p}{u_T} + D = \frac{1}{2}\rho ac\left(\frac{c_d}{a}u_T^2 + u_p u_T\theta - u_p^2\right)$$

Perturbation forces are

$$\delta F_z = \frac{1}{2}\rho ac\left[\delta u_T\left(2u_T\theta - u_p\right) - \delta u_p(u_T) + \delta\theta u_T^2\right]$$

$$\delta F_x = \frac{1}{2}\rho ac\left[\delta u_T\left(2u_T\frac{c_d}{a} + u_p\theta\right) + \delta u_P(u_T\theta - 2u_p) + \delta\theta(u_p u_T)\right]$$

For making analysis simple, the effect of radial force is neglected.

The flow components are

Steady:

$$\begin{aligned}\tfrac{u_T}{\Omega R} &= x + \mu\sin\psi\\ \tfrac{u_p}{\Omega R} &= \lambda + x\dot{\beta} + \beta\mu\cos\psi\end{aligned} \tag{7.6}$$

Perturbation:

$$\begin{aligned}\tfrac{\delta u_T}{\Omega R} &= -x\dot{\zeta} - \mu\zeta\cos\psi\\ \tfrac{\delta u_p}{\Omega R} &= x\dot{\beta} + \mu\beta\cos\psi\end{aligned} \tag{7.7}$$

The solution of the governing equation (7.6) consists of two major steps.

(a) Calculation of trim.

(b) Calculation of perturbation stability.

7.4.1 Perturbation Stability Solution

It is assumed that the flutter motion is a small perturbation about the steady trim solution.

$$(\beta)_{\text{Total}} = (\beta)_{\text{trim}} + (\beta)_{\text{perturbation}}$$

$$(\zeta)_{\text{Total}} = (\zeta)_{\text{perturbation}}$$

This is because $(\zeta)_{\text{trim}}$ trim is neglected. The trim values of β are calculated as

$$(\beta)_{\text{trim}} = -\beta_{1c}\sin\psi + \beta_{1s}\sin\psi = \beta_T$$

$$\overset{*}{(\beta)}_{\text{trim}} = \beta_0 + \beta_{1c}\cos\psi + \beta_{1s}\cos\psi = \overset{*}{\beta}_T$$

Let us remove the perturbation word from β and ζ. Substituting this in the governing equation (7.5), and also including the perturbation aerodynamic moment expressions, and keeping linear terms in perturbation motion components one gets,

$$\begin{bmatrix}\overset{**}{\beta}\\ \overset{**}{\zeta}\end{bmatrix} + [C(\psi)]\begin{bmatrix}\overset{*}{\beta}\\ \overset{*}{\zeta}\end{bmatrix} + [K(\psi)]\begin{bmatrix}\beta\\ \zeta\end{bmatrix} = 0 \tag{7.8}$$

These are matrices of order two, and the various terms are

$$c_{11}(\psi) = \frac{\gamma}{8}(1 + \frac{4}{3}\mu\sin\psi)$$

$$
\begin{aligned}
c_{12}(\psi) &= \frac{\gamma}{8}\left(\frac{4}{3}\lambda + \frac{4}{3}\mu\beta_T\cos\psi + \overset{*}{\beta}_T\right) \\
&\quad -\frac{\gamma}{4}\theta\left(1+\frac{4}{3}\mu\sin\psi\right) + 2\beta_T \\
c_{21}(\psi) &= -\frac{\gamma}{4}\left(\frac{4}{3}\lambda + \frac{4}{3}\mu\beta_T\cos\psi - \overset{*}{\beta}_T\right) \\
&\quad +\frac{\gamma}{8}\theta\left(1+\frac{4}{3}\mu\sin\psi\right) - 2\beta_T \\
c_{22}(\psi) &= \frac{\gamma}{8}\theta\left(\frac{4}{3}\lambda\frac{4}{3}\mu\cos\psi\beta_T + \overset{*}{\beta}_T\right) \\
&\quad +\frac{c_{d_0}}{a}\frac{\gamma}{4}\left(1+\frac{4}{3}\mu\sin\psi\right) - 2\beta_T\,\overset{*}{\beta}_T \\
k_{11}(\psi) &= \nu_\beta^2 + \frac{\gamma}{8}\left(\frac{4}{3}\mu\cos\psi + 2\mu^2\sin\psi\,\cos\psi\right) \\
&\quad -\frac{\gamma}{8}k_{p_\beta}\left(1+\frac{8}{3}\mu\sin\psi + 2\mu^2\sin^2\psi\right) \\
k_{12}(\psi) &= \frac{\gamma}{8}\mu\cos\psi\left(2\lambda + frac43\,\overset{*}{\beta}_T\right) - \frac{\gamma}{4}\theta\left(\frac{4}{3}\mu\cos\psi + 2\mu^2\sin\psi\,\cos\psi\right) \\
&\quad \frac{\gamma}{4}\beta_T\left(\mu^2\cos 2\psi - \frac{2}{3}\mu\sin\psi\right) \\
&\quad -\frac{\gamma}{8}k_{p_\beta}\left(1+\frac{8}{3}\mu\sin\psi + 2\mu^2\sin^2\psi\right) \\
k_{21}(\psi) &= -\frac{\gamma}{4}\mu\cos\psi\left(2\lambda + frac43\,\overset{*}{\beta}_T\right) + \frac{\gamma}{8}\theta\left(\frac{4}{3}\mu\cos\psi + \mu^2\sin 2\psi\right) \\
&\quad -\frac{\gamma}{2}\beta_T\mu^2\cos^2\psi + \frac{\gamma}{8}k_{p_\beta}\left[\frac{4}{3}\lambda\left(1+\frac{3}{2}\mu\sin\psi\right)\right. \\
&\quad \left. + \overset{*}{\beta}_T\left(1+\frac{8}{3}\mu\sin\psi\right) + \beta_T\left(\frac{4}{3}\mu\cos\psi + \mu^2\sin 2\psi\right)\right] \\
k_{22}(\psi) &= \nu_\zeta^2 + \frac{\gamma}{8}\left[2\frac{c_{d_0}}{a}\left(\frac{4}{3}\mu\cos\psi + \psi^2\sin 2\psi\right)\right. \\
&\quad +\mu\cos\psi\,\theta\left(2\lambda + \frac{4}{3}\overset{*}{\beta}_T\right) - \beta_T\theta\left(\frac{4}{3}\mu\sin\psi - 2\mu^2\cos\psi\right) \\
&\quad \left. +2\mu\beta_T\sin\psi\left(2\lambda + \frac{4}{3}\overset{*}{\beta}_T + 2\mu\beta_T\cos\psi\right)\right] \\
&\quad +\frac{\gamma}{8}k_{p_\beta}\left[\frac{4}{3}\lambda\left(1+\frac{3}{2}\mu\sin\psi\right) + \beta_T\left(\frac{4}{3}\mu\cos\psi + \mu^2\sin 2\psi\right)\right. \\
&\quad \left. \overset{*}{\beta}\left(1+\frac{4}{3}\mu\sin\psi\right)\right]
\end{aligned}
$$

In the above expressions

$$\theta = \theta_0 + \theta_{1c}\cos\psi + \theta_{1s}\sin\psi$$

The stability of the system is calculated from the solution of the perturbation equations (7.8). There are many methods to solve these equations. Two possible approaches are discussed here

(a) Constant coefficient approximation.

(b) Floquet Theory.

7.4.2 Constant Coefficient Approximation

The coefficients of the matrices ($\tilde{c}$, $\tilde{k}$) contain periodic terms, and these are approximanted as constant terms by taking average values over a period of 2π. For example,

$$(c_{ij})_{\text{new}} = \frac{1}{2\pi}\int_0^{2\pi} c_{ij}(\psi)\, d\psi$$

$$(k_{ij})_{\text{new}} = \frac{1}{2\pi}\int_0^{2\pi} k_{ij}(\psi)\, d\psi$$

and this results in

$$c_{11} = \frac{\gamma}{8}$$

$$c_{12} = 2\beta_0 + \frac{\gamma}{8}\left(\frac{4}{3}\lambda + \frac{2}{3}\mu\beta_{1c}\right) - \frac{\gamma}{4}\left(\theta_0 + \frac{2}{3}\mu\theta_{1s}\right)$$

$$c_{21} = -2\beta_0 - \frac{\gamma}{4}\left(\frac{4}{3}\lambda + \frac{2}{3}\mu\beta_{1c}\right) + \frac{\gamma}{8}\left(\theta_0 + \frac{2}{3}\mu\theta_{1s}\right)$$

$$c_{22} = \frac{\gamma}{8}\left[2\frac{c_{d_0}}{a} + \frac{1}{2}\theta_{1c}\beta_{1s} - \frac{1}{2}\theta_{1s}\beta_{1c} + \frac{2}{3}\mu\theta_{1c} + \frac{2}{3}\mu\theta_{1c}\beta_0 + \theta_0\left(\frac{4}{3}\lambda + \frac{2}{3}\mu\beta_{1c}\right)\right]$$

$$k_{11} = \nu_\beta^2 - \frac{\gamma}{8}k_{p_\beta}(1+\mu^2)$$

$$k_{12} = -\frac{\gamma}{8}k_{p_\zeta}(1+\mu^2) - \frac{\gamma}{6}\mu\theta_{1c}$$

$$k_{21} = \frac{\gamma}{6}\lambda k_{p_\zeta} + \frac{\gamma}{8}\mu\left(\frac{2}{3}\theta_{1c} - \frac{4}{3}\beta_{1c} - 2\mu\beta_0\right)$$

$$k_{22} = \frac{\gamma}{8}\left[\mu\lambda\theta_{1c} - \frac{2}{3}\mu\beta_0\theta_{1s} - \frac{4}{3}\mu\beta_0\beta_{1c} + 2\mu\lambda\beta_{1s}\right]\frac{\gamma}{6}k_{p_\zeta}\lambda$$

The perturbation equations (7.8) become constant coefficient equations and these can be solved as a standard eigenvalue problem.

7.4.3 Floquet Theory

The perturbation equations (7.8) contain periodic terms and the stability of these equations can be calculated using Floquet theory. As a first step, the Floquet transition matrix is to be calculated. For this purpose, the equatoins (7.8) are transformed to first order form.

$$\{\overset{*}{q}\} = [A(\psi)]\{q\} \tag{7.9}$$

where

$$\{q\} = \begin{bmatrix} \beta \\ \zeta \\ \overset{*}{\beta} \\ \overset{*}{\zeta} \end{bmatrix}$$

$$[A] = \begin{bmatrix} \tilde{O} & \tilde{I} \\ -\tilde{k} & -\tilde{c} \end{bmatrix}$$

To obtain the Floquet transition matrix $[Q]$, the equations (7.9) are solved numerically using some standard time integration technique (say Runge-Kutta) with unity initial conditions. The solution at $\psi = 2\pi$ gives the elements of transistion matrix. For example,

$$\begin{bmatrix} \beta \\ \zeta \\ \overset{*}{\beta} \\ \overset{*}{\zeta} \end{bmatrix} = \begin{bmatrix} 1 \\ 0 \\ 0 \\ 0 \end{bmatrix}_{Ic} \Rightarrow \begin{bmatrix} Q_{11} \\ Q_{21} \\ Q_{31} \\ Q_{41} \end{bmatrix} \text{ (solution at } \psi = 2\pi)$$

After the transition matrix is evaluated, the next step is to obtain its eigenvalue.

$$\lambda\{q\} = [Q]\{q\}$$

If the absolute value of any of the eigenvalue ($\lambda|$) is greater than one, the system is unstable.

The numerical results are obtained for a typical rotor configuration with the following characteristics

$$\begin{array}{cccc} \nu_\beta = 1.15 & \gamma = 1.15 & \frac{c_T}{\sigma} = .2 & \sigma = .05 \\ \nu_\zeta = 1.4 & k_{p_\beta} = k_{p_\zeta} = 0 & \beta_p = 0 & f/A = 0.01 \\ c_{d_0} = .01 & a = 2\pi & \frac{h}{R} = .2 & \end{array}$$

$$x_{cg} = y_{cg} = 0 \qquad c_{m_{xF}} = c_{m_{yF}} = 0$$

Earlier, the trim is calculated for this configuration. These results are plotted for various values of advance ratio μ.

Conclusions:

1. The constant coefficient approximation in the rotating system gives satisfactory results for low advance ratio ($\mu < 0.1$).
2. The flap-lag stability in forward flight is very sensitive to the trim solution. For example, the propulsive trim results are quite different from moment trim results.
3. For large advance ratio ($\mu > 0.1$), the inflow is affected appreciably by the helicopter drag term (f/A).
4. The implicit periodic coefficients (due to β_{1c}, β_{1s}, θ_{1c}, θ_{1s}) and the explicit periodic coefficients ($\mu \sin\psi$, $\mu \cos\psi$) are important for flap-lag stability analysis.
5. The torsion degree of motion has a considerable influence on blade stability if torsional frequency is small.

References

1. Johnson, W., Helicopter Theory, Princeton University Press, 1980, Chapter 12.
2. Biggers, J. C., "Some Approximations to the Flapping Stability of Helicopter Rotors," Journal of the American Helicopter Society, Vol. 19, No. 4, Oct. 1974.
3. Friedman, P. P. and Kattapalli, S. B. R., "Coupled Flap-Lag-Torsional Dynamics of Hingeless Rotor Blades in Forward Flight," Journal of the American Helicopter Society, Vol. 24, No. 4, Oct. 1982, pp. 28-36.

4. Peters, D. A., "Flap-Lag Stability of Helicopter Rotor Blades in Forward Flight," Journal of the American Helicopter Society, Vol. 20, No. 4, Oct. 1975, pp. 2-13.

5. Panda, B. and Chopra, I., "Flap-Lag-Torsion Stability in Forward Flight," Presented at the Second Decennial Specialists' Meeting on Rotorcraft Dynamics at Ames Research Center, Moffett Field, Calif., Nov. 1984.

6. Panda, B. and Chopra, I., "Dynamic Stability of Hingeless and Bearingless Rotors in Forward Flight," Presented at the International Conference on Rotorcraft Basic Research, Research Triangle Park, North Carolina, Feb. 1985.

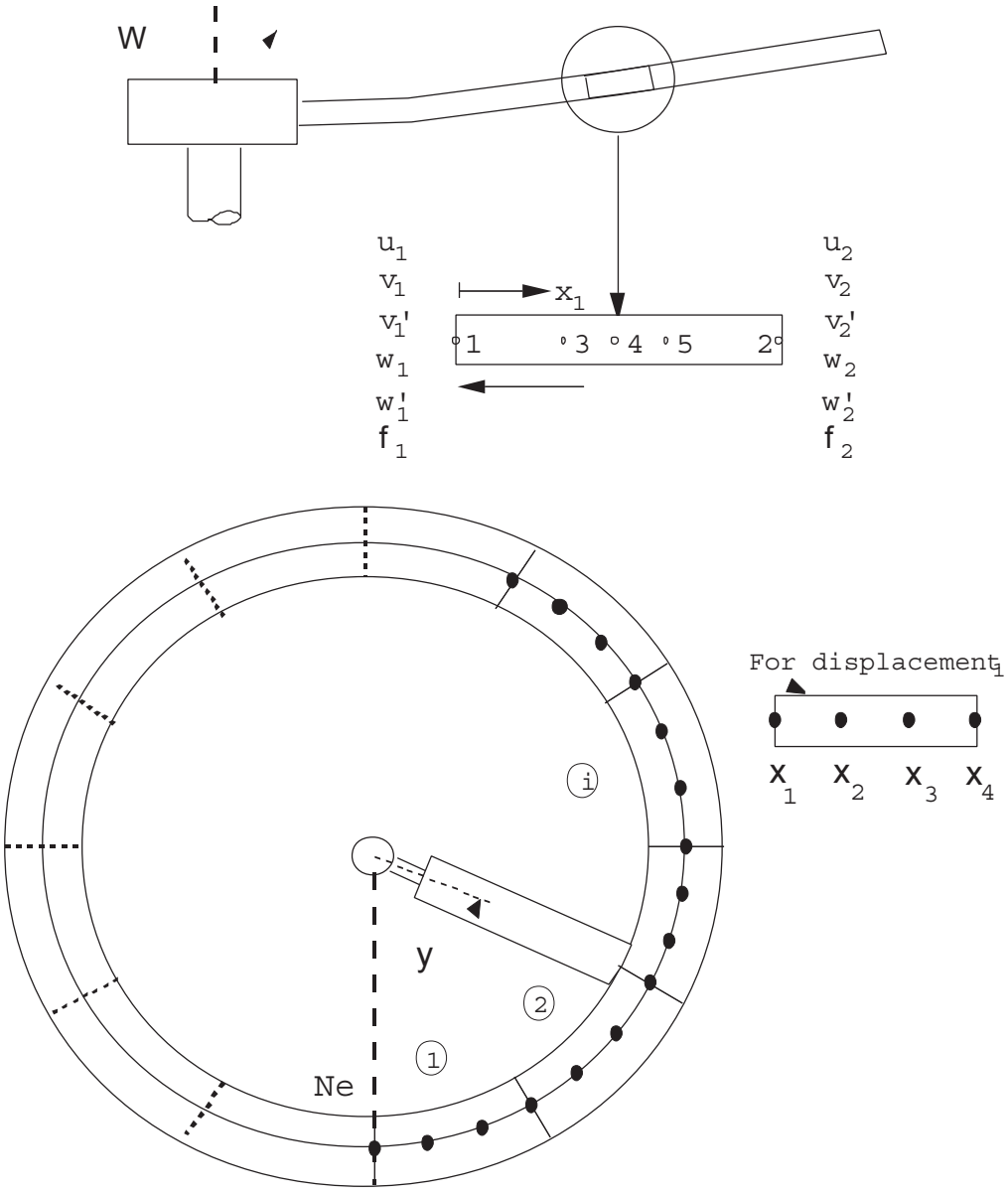

COUPLED TRIM ANALYSIS

- Uncoupled Vehicle Trim (Propulsive)
  - Control Settings and Vehicle Attitude
  - Initial Guess for Iteration Process